Efficient Capture of Carbon Dioxide with Novel Mass-Transfer Intensification Device Using Ionic Liquids

Liang-Liang Zhang, Jie-Xin Wang, Zhi-Ping Liu, and Ying Lu
State Key Laboratory of Organic–Inorganic Composites, Beijing University of Chemical Technology, Beijing 100029, P.R. China

Guang-Wen Chu
Research Center of the Ministry of Education for High Gravity Engineering and Technology, Beijing University of Chemical Technology, Beijing 100029, P.R. China

Wen-Chuan Wang
State Key Laboratory of Organic–Inorganic Composites, Beijing University of Chemical Technology, Beijing 100029, P.R. China

Jian-Feng Chen
State Key Laboratory of Organic–Inorganic Composites, Beijing University of Chemical Technology, Beijing 100029, P.R. China

Research Center of the Ministry of Education for High Gravity Engineering and Technology, Beijing University of Chemical Technology, Beijing 100029, P.R. China

DOI 10.1002/aic.14072
Published online March 14, 2013 in Wiley Online Library (wileyonlinelibrary.com)

A novel mass-transfer intensified approach for CO_2 capture with ionic liquids (ILs) using rotating packed bed (RPB) reactor was presented. This new approach combined the advantages of RPB as a high mass-transfer intensification device for viscous system and IL as a novel, environmentally benign CO_2 capture media with high thermal stability and extremely low volatility. Amino-functionalized IL (2-hydroxyethyl)-trimethyl-ammonium (S)−2-pyrrolidinecarboxylic acid salt ([Choline][Pro]) was synthesized to perform experimental examination of CO_2 capture by chemical absorption. In RPB, it took only 0.2 s to reach 0.2 mol CO_2/mol IL at 293 K, indicating that RPB was kinetically favorable to absorption of CO_2 in IL because of its efficient mass-transfer intensification. The effects of operation parameters on CO_2 removal efficiency and IL absorbent capacity were studied. In addition, a model based on penetration theory was proposed to explore the mechanism of gas–liquid mass transfer of ILs system in RPB. © 2013 American Institute of Chemical Engineers *AIChE J*, 59: 2957–2965, 2013
Keywords: CO_2 capture, ionic liquids, rotating packed bed, modeling

Introduction

CO_2 concentration in the atmosphere associated with energy use has increased by a third over preindustrial levels, from about 280 to 385 ppm,[1] which is main part of the cause of global warming over the past century. With the considerable increase in consumption and demand for fossil fuels, CO_2 will continue to be greatly discharged to the atmosphere, further adding to the global warming.[2,3] Recent estimates by the Intergovernmental Panel on Climate Change indicate that deep reduction from current CO_2 emission will be required by midcentury if we are to stabilize atmospheric CO_2 concentration to limit predicted global average temperature rise.[4,5]

Carbon capture and storage (CCS) technologies are a promising route to achieve a meaningful reduction in CO_2 emissions in the near-term.[5] In a positive scenario, the use of CCS technologies in the power plants would result in a total of 5.1–10.4 Gt of CO_2 being captured.[6] It is accepted that the challenges associated with the transport and storage of such large quantities of CO_2 are nontrivial, but not insurmountable. However, the cost of CO_2 capture will account for more than 80% of the total CCS cost in current analysis, which remains to be a problem.[7] Therefore, it is important to select optimal methods of CO_2 capture in terms of their capital and operation cost. A wide range of approaches, including cryogenic distillation,[8] membrane purification,[9,10] absorption,[11,12] and pressure-swing adsorption,[13–15] have been proposed to capture CO_2. Among these approaches, amine scrubbing is the current state-of-art technology for CO_2 capture at an industrial scale. Although amines, in particular aqueous solutions of monoethanolamine (MEA),

Correspondence concerning this article should be addressed to J.-F. Chen at chenjf@mail.buct.edu.cn.

are effective in capturing CO_2, they suffer from several disadvantages. First of all, when MEA is applied to CO_2 capture in conventional absorber/stripper systems in power plants, the energy consumption is considerable. Improved solvents and process configurations are expected to reduce the cost of CO_2 capture by MEA scrubbing to 30–40 US \$/ton CO_2, but it is still a big challenge to meet the acceptable cost (DOE target < 20 \$/ton CO_2).[7,16] The uptake of the corrosive amine into the gas stream causes serious corrosion in the process infrastructure. The loss of volatile amine necessitates the periodic injection of fresh solution.[17] Furthermore, the thermal instability of both the solvent and the carbonate leads to decomposition, which can cause secondary pollution if there is insufficient containment.[18] Therefore, it is urgent to develop novel and cost-effective solvents that can facilitate the sequestration of CO_2 from the flue gas without concurrent loss of the capture agent into the gas stream. Lots of alternative solvents have been explored to verify the feasibility for commercial deployment.[19–21]

Recently, ionic liquids (ILs) provide a promising new option for CO_2 capture.[22–28] Much of this interest stems from several interesting properties of ILs: high thermal stability, extremely low volatility, good solubility of CO_2, and the ability to manipulate solvent properties through ion selection.[29–33] Intensive efforts have been directed toward the development of ILs because of their numerous advantages. Davis and coworkers reported the first example of the chemical absorption of CO_2 that used an amino-functionalized task-specific IL.[34] Their results showed that 0.5 molar CO_2 could be captured per molar IL with a gravimetric capacity of about 7% for 3 h under ambient pressure. Subsequently, a number of research groups have studied other amino-functionalized ILs for CO_2 capture.[35,36] While currently available ILs display CO_2 solubilities that are approximately the same as molecular organic solvents, the potential for improving these values through modification of the ions making up the solvent promises exciting opportunities for future improvements.[30,37] However, the technical impediment of ILs practical applications is also attracting lots of attention. Usually, most of ILs have enormous viscosities and lack of fluidities, thus, greatly affecting their large-scale application and long-term commercial viability.[34,36,38] In particular, it is hard to achieve practical CO_2 capture applications in conventionally industrial reactors owing to the great mass-transfer resistance and low gas–liquid mass-transfer rate in such high-viscous ILs. Therefore, it is significant to develop a new technology with high mass-transfer efficiency for such high viscous systems and gain the acceptance from an industrial viewpoint.

Rotating packed bed (RPB), also known as Higee (High gravity), has been used as a good gas–liquid contactor or reactor for the applications of reactive precipitation, distillation, stripping, and so forth.[39–45] RPB is designed to generate high acceleration via centrifugal force, leading to the formation of thin liquid films and tiny liquid droplets, which could enhance the mass transfer between gas and liquid.[46,47] It is reported that the mass-transfer coefficient in the RPB is at least one to two order of magnitude higher than that in the conventional packed tower.[48,49] Moreover, a structured packing in RPB is specifically designed to have both a large gas–liquid interfacial area and a low pressure drop.[50] Both of these characteristics reduce the amount of packing required and, thus, minimize the size of the equipment. Handling of high viscous systems in RPB has been reported in our previous work.[51] The volatile organic compound was successfully removed from high viscous syrup by RPB. Its removal efficiency was increased by about 67% compared to a flash tank devolatilizer.[52] Therefore, we believe that RPB is an ideal candidate to intensify the mass transfer in the high viscous systems.

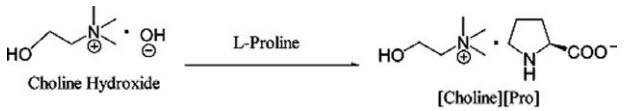

Figure 1. Schematic illustration to synthesize the IL [Choline][Pro].

To overcome the hurdle of ILs as CO_2 capture media for industrial application, an innovate approach is proposed here for large-scale CO_2 capture. This hybrid approach combines the advantage of RPB as a high effective reactor and ILs as novel, environmentally benign CO_2 capture media with high thermal stability and extremely low volatility. Amino-functionalized IL (2-hydroxyethyl)-trimethyl-ammonium (*S*)−2-pyrrolidinecarboxylic acid salt ([Choline][Pro]) is adopted to validate the feasibility and efficiency of this approach. The effects of temperature, RPB rotating speed, gas flow rate, liquid flow rate, and CO_2 content in gas mixture on CO_2 removal efficiency and absorbent capacity are studied. The absorption/desorption process is repeated for several cycles to investigate the regeneration ability of the IL. In addition, a model based on penetration theory is proposed to describe the mechanism of gas–liquid mass transfer of ILs system in the RPB. Further optimization is provided for the process based on the model.

Experimental

IL synthesis and experimental apparatus

Amino-functionalized IL (2-hydroxyethyl)-trimethyl-ammonium (*S*)−2-pyrrolidinecarboxylic acid salt ([Choline][Pro]) is synthesized to perform experimental measurement. It was reported that the IL could absorb as high as 10 wt % CO_2 at room temperature and ambient pressure. The procedure to synthesize the IL [Choline][Pro] was based on the method reported by Han and coworkers,[53] which is schematically illustrated in Figure 1. The IL is obtained by neutralization of choline hydroxide and L-proline and is a light-yellow oil at room temperature. Choline hydroxide solution (ca. 45% molar in methanol) was supplied by Aldrich. L-Proline (99%) was produced by Chinese National Medicine. The chemicals were used as received. The IL was dried under vacuum at 343 K for 48 h before use, and it was collected after experiment and reconditioned for further use. The water content in the IL was less than 0.1 wt %, as measured by Karl Fischer analysis. N_2 with a purity of 99.99% and the gas mixture with CO_2 molar fraction of 10 and 20% were purchased from Beijing Ruyuanruquan Technology, China.

The experimental set-up for CO_2 absorption is schematically shown in Figure 2. The RPB contactor mainly consists of a mesh packing, a liquid inlet, a gas inlet, a liquid outlet, and a gas outlet (see Figure 3). The inner and outer diameters of the rotator are 20 and 60 mm, respectively, and the axial length of the rotator is 20 mm. The bed is packed with stainless wire mesh with porosity and surface area of 0.90 and 850 m^2/m^3, respectively. The packing consists of 11

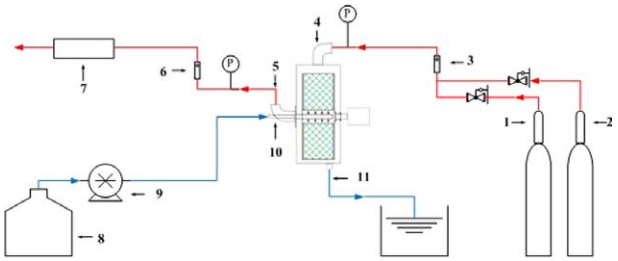

Figure 2. Scheme of experimental set-up. (1) Gas cylinder of N_2, (2) gas cylinder of N_2 and CO_2 gas mixture, (4) gas inlet, (5) gas outlet, (6) gas flowmeter, (7) IR gas analyzer, (8) liquid storage, (9) pump, (10) liquid inlet, and (11) liquid outlet.

[Color figure can be viewed in the online issue, which is available at wileyonlinelibrary.com]

layers. The rotator is installed inside the fixed casing. The inner diameter of the gas pipeline is 12.0 mm. The inner diameter of the liquid pipeline between the liquid storage and the liquid inlet is 5.0 mm. The inner diameter of the liquid pipeline linked with the liquid outlet is 9.0 mm. All the pipelines and equipments are swept by nitrogen prior to use to remove the moisture and air.

CO_2 absorption measurement

During the process, the mixture gas flowed inward from the outer edge of the RPB by a pressure driving force, and the absorbent was pumped from the storage tank to the inner edge of the RPB via three holes (the diameter: 0.5 mm) of the distributor. The velocity of the absorbent solution was observed to be high enough to avoid the entrainment in the discharged gas stream. The absorbent moved outward and left from the outer edge of the RPB via a centrifugal force. Both gas and liquid streams contacted countercurrently in the RPB, in which CO_2 in the gas stream was dissolved and reacted with the absorbent in the liquid stream. The gas

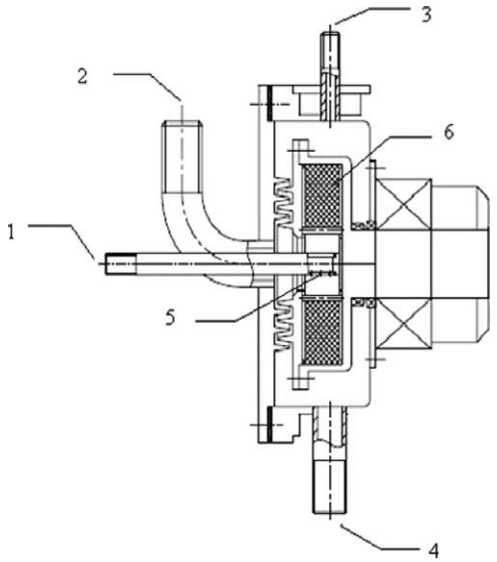

Figure 3. Schematic diagram of RPB for CO_2 absorption. (1) Liquid inlet, (2) gas outlet, (3) gas inlet, (4) liquid outlet, (5) liquid distributor, and (6) mesh packing.

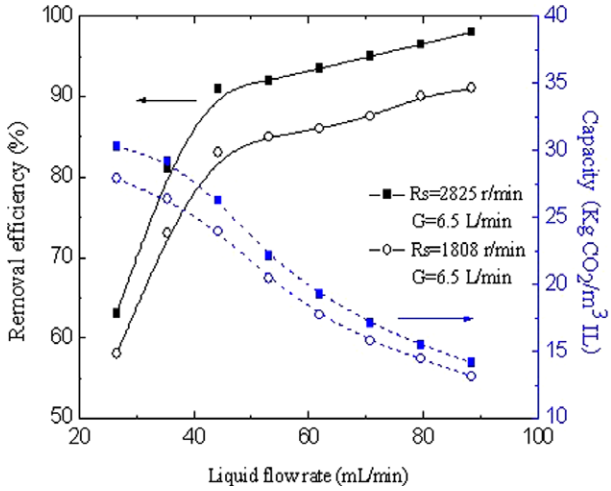

Figure 4. Effect of liquid flow rate on CO_2 removal efficiency and absorbent capacity in RPB.

[Color figure can be viewed in the online issue, which is available at wileyonlinelibrary.com]

leaving the RPB was discharged from the gas outlet of the RPB, whereas the CO_2-rich absorbent was discharged from the liquid outlet of the RPB. After the IL samples absorbed CO_2, they were readily regenerated in a rotary evaporator at 338 K for 3 h, and the working vacuum degree was 0.003 MPa. The regenerated IL was repeatedly used for further absorption experiments. The CO_2 contents in the outlet gas streams were measured by an infrared gas analyzer (GXH-3010F, Huayun Analytical Instrument Institution, China, CO_2 molar fraction ranging from 0 to 20%). The gas tightness was carefully checked to ensure no leakage of the gas before each experiment. The CO_2 removal efficiency η can be calculated from the following equation

$$\eta = \left[1 - \left(\frac{Y_{CO_2,out}}{1-Y_{CO_2,out}}\right)\left(\frac{1-Y_{CO_2,in}}{Y_{CO_2,in}}\right)\right] \times 100\% \qquad (1)$$

In this study, the pressure of inlet gas was maintained at 0.1 MPa. The pressure drop from the inlet to the outlet was always lower than 3 kPa, which could be ignored. To maintain high gravity level, the rotating speed was varied from 1469 to 3842 rpm. All the data were obtained until a steady-state operation was maintained for 2 min.

Results and Discussion

For effective capture of CO_2, the scrubbing approach must have the following features: (1) high CO_2 removal efficiency, (2) large absorbent capacity, (3) fast absorption kinetics, and (4) easy regeneration for absorbent.

CO_2 removal efficiency and absorbent capacity

The CO_2 removal efficiency and absorbent capacity will be discussed first. Figures 4 and 5 exhibit the evolution of CO_2 removal efficiency and absorbent capacity with liquid flow rate and gas flow rate. The influence of liquid flow rate has been investigated at two typical RPB rotating speeds (2825 and 1808 rpm). An increase of liquid flow rate or gas flow rate not only reduces liquid-side or gas-side mass-transfer resistance that could enhance mass transfer but also changes the gas–liquid ratio in RPB, thereby affecting the

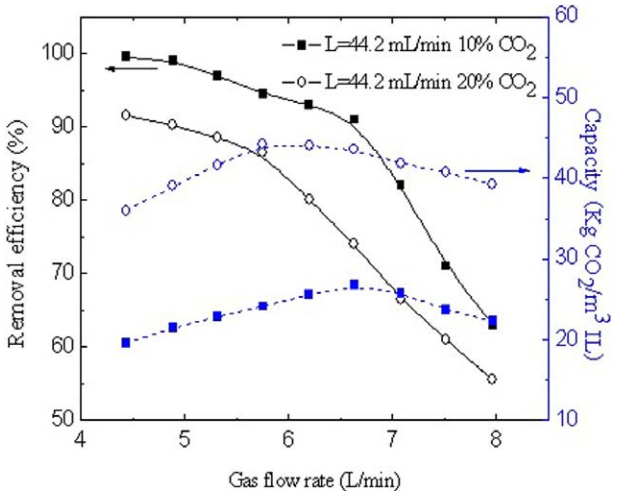

Figure 5. Effect of gas flow rate on CO_2 removal efficiency and absorbent capacity in RPB.

[Color figure can be viewed in the online issue, which is available at wileyonlinelibrary.com]

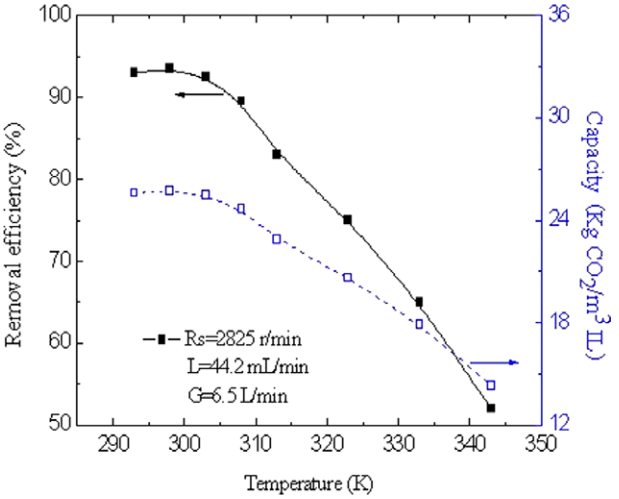

Figure 7. Effect of temperature on CO_2 removal efficiency and absorbent capacity in RPB.

[Color figure can be viewed in the online issue, which is available at wileyonlinelibrary.com]

gas–liquid contact state. Obviously, the removal efficiency maintains a value of higher than 90% as the liquid flow rate is about 45 mL/min, and the gas flow rate is about 6.5 L/min (at the rotating speed of 2825 rpm). Meanwhile, the absorbent capacity could also maintain a high level for 10% CO_2 content (24 kg CO_2/m^3 IL). This is ascribed to the fact that an even distribution of the liquid on the packing could be formed, and a steady effective gas–liquid mass-transfer interface for favorable gas–liquid contact could be, thus, achieved. Besides, with the increase of CO_2 content from 10 to 20% (see Figure 4b), the absorbent capacity varies from 24 kg CO_2/m^3 IL to as high as 43 kg CO_2/m^3 IL, while the CO_2 removal efficiency decreases from 92 to 87%. The increase of the CO_2 content could enhance the absorbent capacity, but it is difficult to remove more CO_2 from the gas stream with a higher CO_2 content within the same contact time as compared to the gas stream with a lower CO_2 content. Therefore, the CO_2 removal efficiency decreases slightly with the increased CO_2 content from 10 to 20%.

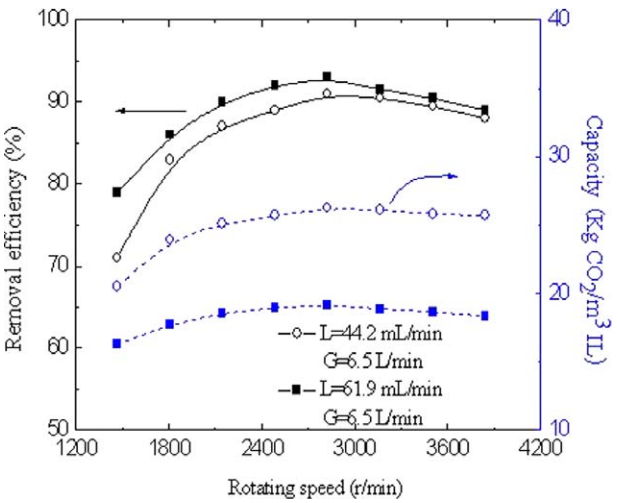

Figure 6. Effect of rotating speed on CO_2 removal efficiency and absorbent capacity in RPB.

[Color figure can be viewed in the online issue, which is available at wileyonlinelibrary.com]

Figure 6 shows the effect of rotating speed on CO_2 removal efficiency and absorbent capacity. It can be clearly seen that CO_2 removal efficiency obviously increases with an increase in the rotating speed ranging from 1100 to 3000 rpm. Vigorous impingement between liquid and packing is achieved with an increase in rotating speed, thereby resulting in a better gas–liquid mass-transfer effect. However, when the rotating speed is further increased, a reverse effect on CO_2 removal efficiency is observed. The possible reason is that the extent of reduction in mass-transfer resistance at a higher rotating speed is compensated by a reduction of the retention time, which is unfavorable to chemical absorption. Furthermore, the trend line of absorbent capacity is similar compared to the trend line of CO_2 removal efficiency. The phenomenon indicates that the rotating speed of 2825 rpm is optimal for our device.

Figure 7 depicts the effect of temperature on the CO_2 removal efficiency and absorbent capacity. With the increase of temperature from 293 to 305 K, CO_2 removal efficiency almost keeps unchanged. However, when the temperature is further increased to 343 K, CO_2 removal efficiency declines dramatically from 93 to 52%. The variation of absorbent capacity is similar to that of removal efficiency. The possible reason is that the increase of temperature would lower the viscosity of IL, leading to the enhancement of CO_2 diffusion in the IL. However, high temperature gives rise to the decrease of reaction equilibrium constant and Henry's law constant for CO_2 absorption, which are dominating factors in the absorption of CO_2 in the IL. Consequently, it is necessary to avoid high temperature for the achievement of high removal efficiencies and absorbent capacities.

Absorption kinetics and regeneration for absorbent

The investigation of CO_2 absorption experiment in a conventional bubble vessel was previously reported.[53] The IL was put in a stainless steel cell (6 mL) at 323 K, and CO_2 of ambient pressure was bubbled through the IL. The conditions of the absorption experiments in RPB and bubble vessel are not consistent, for example, the gas residence time in the bubble vessel is six times higher than that in the RPB, and the temperature in the bubble vessel is higher. In general,

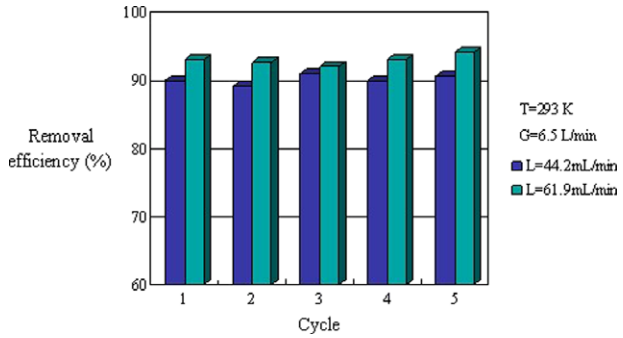

Figure 8. Five cycles of CO_2 absorption/desorption in [Choline][Pro] in RPB.

[Color figure can be viewed in the online issue, which is available at wileyonlinelibrary.com]

the condition in the bubble vessel is more favorable for gas–liquid mass transfer because longer gas residence time means more gas–liquid contact time to achieve mass transfer and higher temperature means lower viscosity. But the absorption of CO_2 was found to be very slow in bubble vessel. The times required to approach 0.2 mol CO_2/mol IL and 0.6 mol CO_2/mol IL were 30 and 240 min, respectively. In RPB, the CO_2 absorption kinetics has been found to be very fast. It took only 0.2 s (calculated by our model) to reach 0.2 mol CO_2/mol IL at 293 K, indicating that RPB was kinetically favorable to the absorption of CO_2 in IL because of its efficient mass-transfer intensification.

To investigate the recycle performance of this IL, CO_2 absorption/desorption experiments were carried out for several cycles. Figure 8 shows the CO_2 removal efficiency of the IL in each cycle. The IL could be used for several times by consecutive absorption/desorption cycles with indetectable losses of performances in RPB, which indicates that the CO_2 removal process is reversible.

Model Development

A model is built to describe the mechanism of gas–liquid mass transfer between CO_2 and IL in the RPB.

Reaction of CO_2 and monoamine-functionalized IL

In the literatures,[53,54] two reaction mechanisms were proposed to explain the [Pro]-anion IL that chemically reacts with CO_2. The reaction of the [Pro]-anion IL with CO_2 through 1:1 mechanism has been confirmed by the spectral analysis in the report of Notre Dame.[54] So this mechanism is adopted in our work, which is shown as followed

$$\mathrm{RNH} + \mathrm{CO_2} \overset{k_{1,IL},K_1}{\leftrightarrow} \mathrm{RNCOO^-} + \mathrm{H^+} \tag{2}$$

where $k_{1,\mathrm{IL}}$ is reaction rate constant of reaction 2, and K_1 is equilibrium constant of reaction 2. RNH represents the monoamine-functionalized IL, $RNCOO^-$ represents the carbamated monoamine-functionalized IL. Reaction 2 is a fast reaction. The overall reaction rate of CO_2 in monoamine-functionalized IL can be expressed in terms of reversible reactions, given by the generally accepted expression

$$r_{\mathrm{ov}} = k_{1,\mathrm{IL}}\, c_{\mathrm{RNH}}\, c_{\mathrm{CO_2}} - \frac{k_{1,\mathrm{IL}}}{K_1} c_{\mathrm{H^+}}\, c_{\mathrm{RNCOO^-}} \tag{3}$$

When a chemical equilibrium is reached for reaction 2, the equilibrium equation can be expressed as

$$k_{1,\mathrm{IL}}\, c_{\mathrm{RNH,eq}}\, c_{\mathrm{CO_2,eq}} = \frac{k_{1,\mathrm{IL}}}{K_1} c_{\mathrm{H^+,eq}}\, c_{\mathrm{RNCOO^-,eq}} \tag{4}$$

where $c_{CO_2,eq}$ is the equilibrium concentration of CO_2. The reaction rate for the reverse reaction can be evaluated by considering equilibrium condition. It is generally true even when the system is not at equilibrium.[55] The net forward rate of the reaction can be deduced from Eq. 4.

$$r_{\mathrm{ov}} = k_{1,\mathrm{IL}}\, c_{\mathrm{RNH}}\, c_{\mathrm{CO_2}} - k_{1,\mathrm{IL}}\, c_{\mathrm{RNH,eq}}\, c_{\mathrm{CO_2,eq}} \tag{5}$$

Using $k_{1,\mathrm{IL}}\, c_{\mathrm{RNH}}\, c_{\mathrm{CO_2}} - k_{1,\mathrm{IL}}\, c_{\mathrm{RNH}}\, c_{\mathrm{CO_2,eq}}$ to substitute $k_{1,\mathrm{IL}}\, c_{\mathrm{RNH}}\, c_{\mathrm{CO_2}} - k_{1,\mathrm{IL}}\, c_{\mathrm{RNH,eq}}\, c_{\mathrm{CO_2,eq}}$ will not effect the calculation of r_{ov}, because $k_{1,\mathrm{IL}}\, c_{\mathrm{RNH}}\, c_{\mathrm{CO_2}}$ is determined in r_{ov} (c_{RNH} is larger than $c_{\mathrm{RNH,eq}}$ and $c_{\mathrm{CO_2}}$ is much large than $c_{\mathrm{CO_2,eq}}$). So Eq. 5 could be rewritten as

$$r_{\mathrm{ov}} = k_{1,\mathrm{IL}} c_{\mathrm{RNH}} c_{\mathrm{CO_2}} - k_{1,\mathrm{IL}} c_{\mathrm{RNH}} c_{\mathrm{CO_2,eq}} = k_{1,\mathrm{IL}} c_{\mathrm{RNH}} \left(c_{\mathrm{CO_2}} - c_{\mathrm{CO_2,eq}}\right) \tag{6}$$

where $c_{\mathrm{CO_2,eq}}$ can be calculated from reaction 1, and written as

$$c_{\mathrm{CO_2,eq}} = \frac{c_{\mathrm{H^+,eq}}\, c_{\mathrm{RNCOO^-,eq}}}{K_1 c_{\mathrm{RNH,eq}}} \tag{7}$$

The overall balance for monoamine-functionalized IL is

$$c_{\mathrm{RNH,total}} = c_{RNH} + c_{\mathrm{RNCOO^-}} \tag{8}$$

From Eq. 6, the overall reaction rate constant k_{ov} is given by the following expression

$$k_{\mathrm{ov}} = k_{1,\mathrm{IL}}\, c_{\mathrm{RNH}} \tag{9}$$

Modeling of the CO_2 absorption in RPB

Before establishing a model for the absorption process, the following assumptions are adopted:

1. According to the study of Basic and Ramshaw and Guo Kai, the liquid flow in RPB has been assumed to be laminar film flow. Majorities of the liquid in the RPB exist in the form of liquid film, where the mass transfer takes place.[46,56] The surface areas of packing are regarded as the gas–liquid effective interfacial area.
2. The rotor in RPB consists of 11 layers of packing. Liquid films are renewed every time it passes through one layer of packing. Figure 9 illustrates the sketch of the wire-mesh packing. The mean lifetime of liquid film in each layer is the same and determined by both liquid residence time and total number of packing layers.

c_{RNH} and $c_{\mathrm{RNCOO^-}}$ can be assumed as a constant at fixed temperature in each liquid film. Consequently, the equilibrium concentration of CO_2 can be treated as a constant. k_{ov} can also be assumed as a constant. The partial different equation describing the diffusion of CO_2 into liquid film accompanied by the pseudo-first-order reversible chemical reaction is

$$\frac{\partial c_{\mathrm{CO_2}}}{\partial t} = D_{\mathrm{CO_2}} \frac{\partial^2 c_{\mathrm{CO_2}}}{\partial x^2} - k_{\mathrm{ov}} \left(c_{\mathrm{CO_2}} - c_{\mathrm{CO_2,eq}}\right), \quad 0 < x < \infty,$$
$$t > 0 \quad B.C. \quad c_{\mathrm{CO_2}}(0,t) = c_{\mathrm{CO_2,0}}, \quad c_{\mathrm{CO_2}}(\infty,t) \le c_{\mathrm{CO_2,eq}} \tag{10}$$

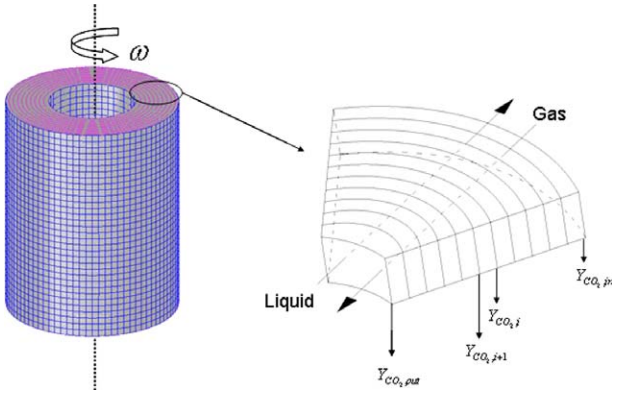

Figure 9. Sketch of a wire-mesh packing.

[Color figure can be viewed in the online issue, which is available at wileyonlinelibrary.com]

$c_{CO_2,0}$, determined by $(pY_{CO_2,i})/(H_{CO_2})$, is the concentration at the gas–liquid interface. Although $c_{CO_2,0}$ is mutative in the packing, it can be regarded as a constant in one layer of the packing (see Figure 9). $c_{CO_2,eq}$ is the equilibrium concentration of CO_2 in the reaction.

Letting $c_A = c_{CO_2} - c_{CO_2,eq}$ and using Laplace transform, we obtain an ordinary differential equation.

$$D_{CO_2}\frac{d^2\tilde{c}_A}{d\tilde{x}^2} - (s + k_{ov})\tilde{c}_A = 0$$
$$B.C. \quad \tilde{c}_A(0,s) = \frac{c_{CO_2} - c_{CO_2,eq}}{s}, \quad \tilde{c}_A(\infty,s) \le 0 \tag{11}$$

The solution to Eq. 11 is

$$\tilde{c}_A(x,s) = \frac{c_{CO_2,0} - c_{CO_2,eq}}{s}\exp\left(-x\sqrt{\frac{s+k_{ov}}{D_{CO_2}}}\right) \tag{12}$$

Using Laplace inverse transform, we obtain an analytical expression for the concentration distribution of CO_2 as a function of time and depth in the liquid film.

$$c_{CO_2} = \frac{c_{CO_2,0} - c_{CO_2,eq}}{s}\exp\left(-x\sqrt{\frac{k_{ov}}{D_{CO_2}}}\right) erfc\left(\frac{x}{2\sqrt{D_{CO_2}t}} - k_{ov}\right) + \frac{c_{CO_2,0} - c_{CO_2,eq}}{s}\exp\left(x\sqrt{\frac{k_{ov}}{D_{CO_2}}}\right) erfc\left(\frac{x}{2\sqrt{D_{CO_2}t}} + k_{ov}\right) + c_{CO_2,eq} \tag{13}$$

where erfc(x) is the excess error function. The mass-transfer rate at the gas–liquid interface is calculated by the first Fick law, given by

$$R_{CO_2} = -D_{CO_2}\frac{\partial c_{CO_2}}{\partial x}|_{x=0} = (c_{CO_2} - c_{CO_2,eq}) \times \left[\sqrt{\frac{D_{co_2}}{\pi t}}\exp(-k_{ov}t) + \sqrt{k_{ov}D_{CO_2}}erf\left(\sqrt{k_{ov}t}\right)\right] \tag{14}$$

where erf(x) is the error function. The liquid film is renewed, when it passes through the packing layer and the renewal frequency is determined by[47]

$$S = u\frac{N_s}{R_1 - R_2} \tag{15}$$

where N_s is the number of layers of the wire-meshed packing, 11 in our study, while R_2 and R_1 are outer and inner radii of the packing, respectively. The u is the average radial flow rate of the liquid film.

$$u = 0.0217L^{0.2279}\left(\omega^2 R\right)^{0.5448} \tag{16}$$

where L is liquid flux. Then, the mean lifetime of the liquid film could be described as follows

$$\bar{t} = \frac{1}{S} \tag{17}$$

According to the assumption that the lifetime of the liquid film on each packing layer is the same, the Higbie age distribution function of mass transfer in the liquid film is, thus, defined as

$$\psi(t) = \frac{1}{\bar{t}}, \quad 0 < t < \bar{t} \tag{18}$$

From Eqs. 14 and 18, the expression of the time-averaged mass-transfer rate of CO_2 per unit interfacial area can be written as

$$\bar{N}_{CO_2} = \int_0^{\bar{t}} R_{CO_2} \times \psi(t)\mathrm{d}t = \frac{\sqrt{k_{ov}D_{CO_2}}}{\bar{t}} \times \left[\bar{t}erf\left(\sqrt{k_{ov}\bar{t}}\right) + \sqrt{\frac{\bar{t}}{\pi k_{ov}}}\exp(-k_{ov}\bar{t}) + \frac{1}{2k_{ov}}erf\left(\sqrt{k_{ov}\bar{t}}\right)\right] \times \left(c_{CO_2,0} - c_{CO_2,eq}\right) \tag{19}$$

where Eq. 19 can also be written as the following one, including the liquid side mass-transfer coefficient (k_L)

$$\bar{N}_{CO_2} = k_L\left(c_{CO_2,0} - c_{CO_2,eq}\right)^L \tag{20}$$

$$k_L = \frac{\sqrt{k_{ov}D_{CO_2}}}{\bar{t}} \times \left[\bar{t}erf\left(\sqrt{k_{ov}\bar{t}}\right) + \sqrt{\frac{\bar{t}}{\pi k_{ov}}}\exp(-k_{ov}\bar{t}) + \frac{1}{2k_{ov}}erf\left(\sqrt{k_{ov}\bar{t}}\right)\right] \tag{21}$$

Based on the study of absorption of CO_2 in MDEA by Qian, $c_{CO_2,0}$ is at least three order of magnitude higher than $c_{CO_2,eq}$, so $c_{CO_2,eq}$ can be ignored in the calculation process of $\bar{N}_{CO_2}$ in Eq. 20.[57]

The surface areas of the packing are regarded as the gas–liquid effective interfacial area. The CO_2 content in the mixture gas leaving this layer of the packing can be calculated as follows

$$Y_{CO_2,i+1} = \frac{GY_{CO_2,i} - \bar{N}_{CO_2}V_t a_t V_m}{G - \bar{N}_{CO_2}V_t a_t V_m} \tag{22}$$

where $\bar{N}_{CO_2}$ is the mass-transfer rate of CO_2 per unit interfacial area, whereas V_t is the volume of the packing, and a_t is the specific area of the packing. $V_t a_t$ is used to calculate the gas–liquid interfacial area in the layer of the RPB, and $\bar{N}_{CO_2}V_t a_t V_m$ is used to approximately calculate the absorption rate of CO_2 in the packing.

As the CO_2 concentration at the inner edge, where the mixture gas enters the RPB, is known, we could compute

Table 1. Physical Properties of [Choline][Pro] at 293 K

μ (Pa s, 293 K)	D (10^{-11} m^2/s, 293 K)	H (MPa, 293 K)	ρ (kg/m^3, 293 K)	T_g (K)	T_m (K)	C^{54} (kg CO_2/m^3 IL, 0.1 MPa)
1.935	1.058	3	1130	202	261	228.1

the CO_2 concentration layer by layer until the gas outlet by Eqs. 10–22. Then, the CO_2 removal efficiency η is obtained.

The physical properties of [Choline][Pro] are presented in Table 1. The viscosity was measured by a viscometer (Haake-rs-150) in this work. This IL is proved to be a Newtonian fluid with various viscosities dependent on temperature. The density is taken from the data reported by Han and coworkers.[58] The diffusion coefficient of CO_2 in [Choline][Pro] is estimated based on the report of Shiflett and Yokozeki using the Stokes–Einstein equation.[25] The Henry's law constant is estimated from the data reported by Liu and coworkers.[24] The glass transition temperature and melting temperature were measured by a differential scanning calorimeter from Mettler Toledo (model DSC822e). The theoretical CO_2 absorbent capacity of the IL is calculated based on the 1:1 reaction mechanism. The physical absorption of CO_2 in the IL is ignored, because it is less than 3% of the overall capacity at 1 bar and 298 K.[54] The reaction kinetics parameter k_{ov} is from our experiment data. Figure 10

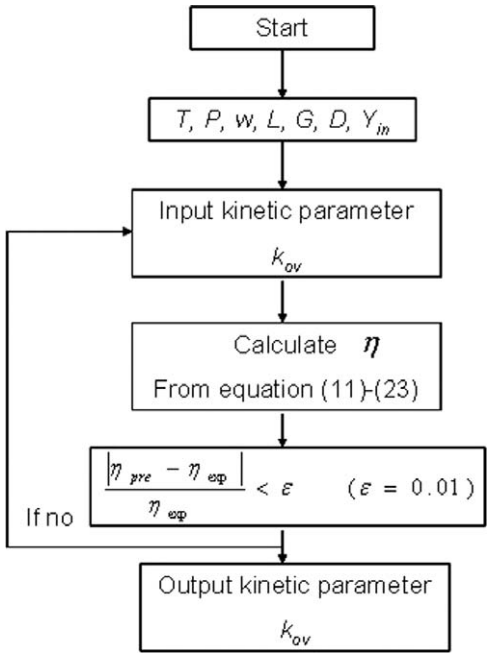

Figure 10. Flow chart of kinetic parameter calculation.

Table 2. The Obtained Values of k_{ov} Parameter at Different Operating Conditions

Rotating Speed (rpm)	Liquid Flow Rate (mL/min)	Gas Flow Rate (L/min)	CO_2 Content (vol %)	Obtained k_{ov} (10^5 1/s)
1469	44.2	6.5	10	1.183
1808	44.2	6.5	10	1.362
2147	44.2	6.5	10	1.518
2486	44.2	6.5	10	1.743
2825	44.2	6.5	10	2.028
3164	44.2	6.5	10	1.950
3503	44.2	6.5	10	1.808
3842	44.2	6.5	10	1.625
2825	26.5	6.5	10	1.012
2825	35.4	6.5	10	1.453
2825	44.2	6.5	10	2.028
2825	53.1	6.5	10	2.202
1808	62.0	6.5	10	1.422
1808	70.8	6.5	10	1.570
1808	79.6	6.5	10	1.876
1808	88.5	6.5	10	2.028
2825	44.2	4.4	10	3.031
2825	44.2	5.3	10	2.366
2825	44.2	6.2	10	2.189
2825	44.2	7.1	10	1.823
2825	44.2	8.0	10	1.689
2825	44.2	4.8	20	2.165
2825	44.2	5.8	20	2.255
2825	44.2	6.6	20	1.842
2825	44.2	7.5	20	1.573

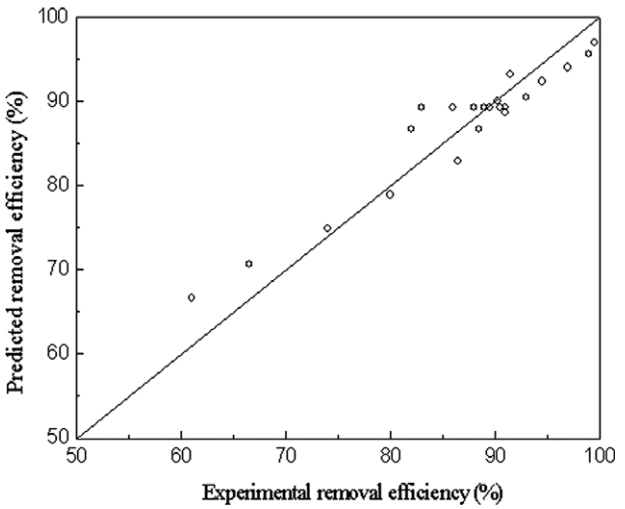

Figure 11. Comparison of predicted and experimental CO_2 removal efficiency.

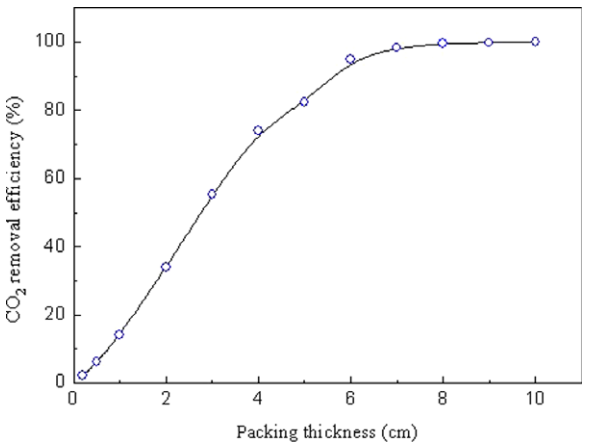

Figure 12. Effect of the packing thickness of RPB on CO_2 removal efficiency.

[Color figure can be viewed in the online issue, which is available at wileyonlinelibrary.com]

illustrates the calculation process of the reaction kinetics parameter k_{ov}. The obtained values of k_{ov} parameter at different operating conditions are shown in Table 2.

A comparison analysis was performed between the experimental data and the calculated data, and the results are shown in Figure 11. It can be clearly seen that the predicted results have a good agreement with the experimental data with a deviation of 10%. The experimental results well verify the accuracy of the model.

In a real process, a high absorbent capacity is usually needed to reduce the cyclic amount of the absorbent and the consequent cost. Therefore, further intensification of gas–liquid mass transfer in RPB should be considered. In this case, increasing the packing thickness of RPB, which could increase the renewal of the liquid film, will be an effective way. Consequently, the gas flow rate could also be increased, thereby providing more CO_2 for absorption. For the above-mentioned model, the optimum packing thickness for RPB can also be predicted. When the liquid flow rate and the gas flow rate increase to 88.5 mL/min and 30 L/min, respectively, Figure 12 displays the dependence of CO_2 removal efficiency on the packing thickness. When the packing thickness is enlarged to 6 cm, the CO_2 removal efficiency is predicted to be more than 90%. More importantly, the apparent absorbent capacity will be increased to be as high as 84 kg CO_2/m^3 IL (0.369 mol CO_2/mol IL), which is promising for real applications.

Conclusions

In summary, we have demonstrated a new approach for CO_2 capture for large-scale industrial application using RPB as absorber with IL as absorbent. The CO_2 absorption efficiency, kinetics, and regeneration of the absorbent were investigated. The results of our study show that the absorption rate is very fast in RPB and RPB is kinetically favorable to the absorption of CO_2 in IL. A model based on penetration theory was built to explore the mechanism of gas–liquid mass transfer between CO_2 and IL system in RPB. Specifically, the results optimized by our model calculation show an exceptionally high capacity to capture CO_2 at room temperature (0.369 mol CO_2/mol IL). This remarkable absorbent capacity is principally due to the high mass-transfer intensification in the RPB.

Acknowledgments

This work was financially supported by National Natural Science Foundation of China (Nos. 21121064, 20990221, 21176009, and 21176013) and National "973" Program of China (No. 2009CB219903). The authors are thankful to Prof. Buxing Han in Institute of Chemistry (Chinese Academy of Science) for kind help on the preparation of ionic liquids and to Prof. David Wong in National Tsing Hua University (Taiwan) for useful discussion on the topic of carbon dioxide capture.

Notation

Y = molar fraction of CO_2 in gas phase,
D = diffusion coefficient, m^2/s
H = Henry's law constant, MPa
V_m = average gas molar volume, L/mol
V_t = the total volume of the packing, m^3
k_L = liquid side mass-transfer coefficient, m/s
L = liquid flux, m^3/m^2 s
N_s = number of layers of the wire-meshed packing
N = time-averaged mass-transfer rate of CO_2 per unit interfacial area, mol/m^2 s
P = total pressure of the gas phase, MPa
S = renewal frequency, s^{-1}
G = total gas flow rate, L/min
T_g = glass transition temperature, K
T_m = melting temperature, K
C = theoretical CO_2 absorbent capacity in the IL, kg CO_2/m^3 IL
u = liquid velocity, m/s
c = concentration, mol/m^3
R = radius of the packed rotator, m
R_1 = radius of the outer packed rotator, m
R_2 = radius of the inner packed rotator, m
R_s = rotating speed of the RPB, rpm
s = complex variable
$\bar{t}$ = mean lifetime of the liquid film, s
k_{ov} = overall pseudo-first-order reaction rate constant, 1/s
$k_{1,II}$ = reaction rate constant of reaction 1, m^3/mol s
K_1 = equilibrium constant of reaction 1
K_2 = equilibrium constant of reaction 2, m^3/mol

Greek letters

η = CO_2 removal efficiency
w = angular velocity, rad/s
α_t = specific area of the packing, m^2/m^3
u = viscosity, Pa/s
ρ = density of the IL, kg/m^3

Subscripts

CO_2 = the data of carbon dioxide
i = the ith layer from the gas inlet
eq = equilibrium
pre = predicted data
exp = experimental data
out = the outlet region of RPB
in = the inlet region of RPB

Abbreviations

RNH = [Choline][Pro]
$RNCOO^-$ = carbamated [Choline][Pro]

Literature Cited

1. Orr FM. CO_2 capture and storage: are we ready? *Energy Environ Sci*. 2009;2:449–458.
2. Keith DW. Why capture CO_2 from the atmosphere? *Science*. 2009;325:1654–1655.
3. Schrag DP. Storage of carbon dioxide in offshore sediments. *Science*. 2009;325:1658–1659.
4. Haszeldine RS. Carbon capture and storage: how green can black be? *Science*. 2009;325:1647–1652.
5. Stone EJ, Lowe JA, Shine KP. The impact of carbon capture and storage on climate. *Energy Environ Sci*. 2009;2:81–91.
6. MacDowell N, Florin N, Buchard A, Hallett J, Galindo A, Jackson G, Adjiman CS, Williams CK, Shah N, Fennell P. An overview of CO_2 capture technologies. *Energy Environ Sci*. 2010;3:1645–1669.
7. Rochelle GT. Amine scrubbing for CO_2 capture. *Science*. 2009;325:1652–1654.
8. Qi GG, Wang YB, Estevez L, Duan XN, Anako N, Park A, Li W, Jones CW, Giannelis EP. High efficiency nanocomposite sorbents for CO_2 capture based on amine-functionalized mesoporous capsules. *Energy Environ Sci*. 2011;4:444–452.
9. Eisaman MD, Alvarado L, Larner D, Wang P, Garg B, Littau KA. CO_2 separation using bipolar membrane electrodialysis. *Energy Environ Sci*. 2011;4:1319–1328.
10. Xiao YC, Chung TS. Grafting thermally labile molecules on cross-linkable polyimide to design membrane materials for natural gas purification and CO_2 capture. *Energy Environ Sci*. 2011;4:201–208.
11. Barzagli F, Mani F, Peruzzini M. Continuous cycles of CO_2 absorption and amine regeneration with aqueous alkanolamines: a comparison of the efficiency between pure and blended DEA, MDEA and

AMP solutions by C-13 NMR spectroscopy. *Energy Environ Sci*. 2010;3:772–779.
12. Puxty G, Rowland R, Allport A, Yang Q, Bown M, Burns R, Maeder M, Attalla M. Carbon dioxide postcombustion capture: a novel screening study of the carbon dioxide absorption performance of 76 amines. *Environ Sci Technol*. 2009;43:6427–6433.
13. Rainbolt JE, Koech PK, Yonker CR, Zheng F, Main D, Weaver ML, Linehan JC, Heldebrant DJ. Anhydrous tertiary alkanolamines as hybrid chemical and physical CO_2 capture reagents with pressure-swing regeneration. *Energy Environ Sci*. 2011;4:480–484.
14. Simmons JM, Wu H, Zhou W, Yildirim T. Carbon capture in metal-organic frameworks—a comparative study. *Energy Environ Sci*. 2011;4:2177–2185.
15. Presser V, McDonough J, Yeon SH, Gogotsi Y. Effect of pore size on carbon dioxide sorption by carbide derived carbon. *Energy Environ Sci*. 2011;4:3059–3066.
16. Figueroa JD, Fout T, Plasynski S, McIlvried H, Srivastava RD. Advances in CO_2 capture technology—the U.S. department of energy's carbon sequestration program. *Int J Greenhouse Gas Control*. 2008;2:9–20.
17. Reza J, Trejo A. Degradation of aqueous solutions of alkanolamine blends at high temperature, under the presence of CO_2 and H_2S. *Chem Eng Commun*. 2006;193:129–138.
18. Veltman K, Singh B, Hertwich EG. Human and environmental impact assessment of postcombustion CO_2 capture focusing on emissions from amine-based scrubbing solvents to air. *Environ Sci Technol*. 2010;44:1496–1502.
19. Zeman F. Experimental results for capturing CO_2 from the atmosphere (R&D note). *AIChE J*. 2008;54:1396–1399.
20. Yi F, Zou HK, Chu GW, Shao L, Chen JF. Modeling and experimental studies on absorption of CO_2 by Benfield solution in rotating packed bed. *Chem Eng J*. 2009;145:377–384.
21. Puxty G, Rowland R. Modeling CO_2 mass transfer in amine mixtures: PZ-AMP and PZ-MDEA. *Environ Sci Technol*. 2011;45:2398–2405.
22. Shiflett MB, Drew DW, Cantini RA, Yokozeki A. Carbon dioxide capture using ionic liquid 1-butyl-3-methylimidazolium acetate. *Energy Fuel*. 2010;24:5781–5789.
23. Wappel D, Gronald G, Kalb R, Draxler J. Ionic liquids for post-combustion CO_2 absorption. *Int J Greenhouse Gas Control*. 2010;4:486–494.
24. Zhang XC, Liu ZP, Wang WC. Screening of ionic liquids to capture CO_2 by COSMO-RS and experiments. *AIChE J*. 2008;54:2717–2728.
25. Shiflett MB, Yokozeki A. Solubilities and diffusivities of carbon dioxide in ionic liquids: [bmim][PF_6] and [bmim][BF_4]. *Ind Eng Chem Res*. 2005;44:4453–4464.
26. Shiflett MB, Yokozeki A. Solubility of CO_2 in room temperature ionic liquid [hmim][Tf_2N]. *J Phys Chem B*. 2007;111:2070–2074.
27. Harris KR, Woolf LA, Kanakubo M. Temperature and pressure dependence of the viscosity of the ionic liquid 1-butyl-3-methylimidazolium hexafluorophosphate. *J Chem Eng Data*. 2005;50:1777–1782.
28. Zhang SJ, Chen YH, Li FW, Lu XM, Dai WB, Mori R. Fixation and conversion of CO_2 using ionic liquids. *Catal Today*. 2006;115:61–69.
29. Chen Y, Hu Z, Gupta KM, Jiang J. Ionic liquid/metal–organic framework composite for CO_2 capture: a computational investigation. *J Phys Chem C*. 2011;115:21736–21742.
30. Camper D, Bara JE, Gin DL, Noble RD. Room-temperature ionic liquid amine solutions: tunable solvents for efficient and reversible capture of CO_2. *Ind Eng Chem Res*. 2008;47:8496–8498.
31. Wang CM, Luo HM, Jiang DE, Li HR, Dai S. Carbon dioxide capture by superbase-derived protic ionic liquids. *Angew Chem Int Ed*. 2010;49:5978–5981.
32. Gonzalez-Miquel M, Palomar J, Omar S, Rodriguez F. CO_2/N_2 selectivity prediction in supported ionic liquid membranes (SILMs) by COSMO-RS. *Ind Eng Chem Res*. 2011;50:5739–5748.
33. Supasitmongkol S, Styring P. High CO_2 solubility in ionic liquids and a tetraalkylammonium-based poly(ionic liquid). *Energy Environ Sci*. 2010;3:1961–1972.
34. Bates ED, Mayton RD, Ntai I, Davis JH. CO_2 capture by a task-specific ionic liquid. *J Am Chem Soc*. 2002;124:926–927.
35. Wang CM, Luo HM, Luo XY, Li HR, Dai S. Equimolar CO_2 capture by imidazolium-based ionic liquids and superbase systems. *Green Chem*. 2010;12:2019–2023.
36. Wang G, Hou W, Xiao F, Geng J, Wu Y, Zhang Z. Low-viscosity triethylbutylammonium acetate as a task-specific ionic liquid for reversible CO_2 absorption. *J Chem Eng Data*. 2011;56:1125–1133.
37. Babarao R, Dai S, Jiang D. Understanding the high solubility of CO_2 in an ionic liquid with the tetracyanoborate anion. *J Phys Chem B*. 2011;115:9789–9794.
38. Gutowski KE, Maginn EJ. Amine-functionalized task-specific ionic liquids: a mechanistic explanation for the dramatic increase in viscosity upon complexation with CO_2 from molecular simulation. *J Am Chem Soc*. 2008;130:14690–14704.
39. Chen YS, Liu HS. Absorption of VOCs in a rotating packed bed. *Ind Eng Chem Res*. 2002;41:1583–1588.
40. Zhao H, Shao L, Chen JF. High-gravity process intensification technology and application. *Chem Eng J*. 2010;156:588–593.
41. Chen J, Li WJ. Hydrothermal synthesis of high densified CdS polycrystalline microspheres under high gravity. *Chem Eng J*. 2011;168:903–908.
42. Lin CC, Su YR. Performance of rotating packed beds in removing ozone from gaseous streams. *Sep Purif Technol*. 2008;61:311–316.
43. Lu XW, Wu W, Chen JF, Zhang PY, Zhao YB. Preparation of polyaniline nanofibers by high gravity chemical oxidative polymerization. *Ind Eng Chem Res*. 2011;50:5589–5595.
44. Chen JF, Shao L, Guo F, Wang XM. Synthesis of nano-fibers of aluminum hydroxide in novel rotating packed bed reactor. *Chem Eng Sci*. 2003;58:569–575.
45. Sun BC, Wang XM, Chen JM, Chu GW, Chen JF, Shao L. Synthesis of nano-$CaCO_3$ by simultaneous absorption of CO_2 and NH_3 into $CaCl_2$ solution in a rotating packed bed. *Chem Eng J*. 2011;168:731–736.
46. Guo K, Guo F, Feng Y, Chen JF, Zheng C, Gardner NC. Synchronous visual and RTD study on liquid flow in rotating packed-bed contactor. *Chem Eng Sci*. 2000;55:1699–1706.
47. Yang K, Chu GW, Zou HK, Sun BC, Shao L, Chen JF. Determination of the effective interfacial area in rotating packed bed. *Chem Eng J*. 2011;168:1377–1382.
48. Chen YS. Correlations of mass transfer coefficients in a rotating packed bed. *Ind Eng Chem Res*. 2011;50:1778–1785.
49. Yang HJ, Chu GW, Xiang Y, Chen JF. Characterization of micromixing efficiency in rotating packed beds by chemical methods. *Chem Eng J*. 2006;121:147–152.
50. Lin CC, Chen BC. Characteristics of cross-flow rotating packed beds. *J Ind Eng Chem*. 2008;14:322–327.
51. Chen JF, Gao H, Zou HK, Chu GW, Zhang L, Shao L, Xiang Y, Wu YX. Cationic polymerization in rotating packed bed reactor: experimental and modeling. *AIChE J*. 2010;56:1053–1062.
52. Li WY, Wu W, Zou HK, Chu GW, Shao L, Chen JF. Process intensification of VOC removal from high viscous media by rotating packed bed. *Chin J Chem Eng*. 2009;17:389–393.
53. Li XY, Hou MQ, Zhang ZF, Han BX, Yang GY, Wang XL, Zou LZ. Absorption of CO_2 by ionic liquid/polyethylene glycol mixture and the thermodynamic parameters. *Green Chem*. 2008;10:879–884.
54. Gurkan BE, de la Fuente JC, Mindrup EM, Ficke LE, Goodrich BF, Price EA, Schneider WF, Brennecke JF. Equimolar CO_2 absorption by anion-functionalized ionic liquids. *J Am Chem Soc*. 2010;132:2116–2117.
55. Qian Z, Xu LB, Cao HB, Guo K. Modeling study on absorption of CO_2 by aqueous solutions of N-methyldiethanolamine in rotating packed bed. *Ind Eng Chem Res*. 2009;48:9261–9267.
56. Burns JR, Ramshaw C. Process intensification: visual study of liquid maldistribution in rotating packed beds. *Chem Eng Sci*. 1996;51:1347–1352.
57. Qian Z, Xu LB, Li ZH, Li H, Guo K. Selective absorption of H_2S from a gas mixture with CO_2 by aqueous N-methyldiethanolamine in a rotating packed bed. *Ind Eng Chem Res*. 2010;49:6196–6203.
58. Hu SQ, Jiang T, Zhang ZF, Zhu AL, Han BX, Song JL, Xie Y, Li WJ. Functional ionic liquid from biorenewable materials: synthesis and application as a catalyst in direct aldol reactions. *Tetrahedron Lett*. 2007;48:5613–5617.

Manuscript received Jun. 4, 2012, revision received Dec. 12, 2012, and final revision received Feb. 18, 2013.